Research Square

Preprints are preliminary reports that have not undergone peer review.
They should not be considered conclusive, used to inform clinical practice,
or referenced by the media as validated information.

Adsorbate-induced Active Site in Zeolite

Guangchao Li
University of Oxford https://orcid.org/0000-0001-7521-8336
Christopher Foo
University of Oxford
Xianfeng Yi
Wuhan Institute of Physics and Mathematics https://orcid.org/0000-0001-9224-3111
Wei Chen
State Key Laboratory of Magnetic Resonance and Atomic and Molecular Physics, National Center for Magnetic Resonance in Wuhan, Key Laboratory of Magnetic Resonance in Biological Systems, Wuhan Institut https://orcid.org/0000-0002-8955-9497
Pu Zhao
University of Oxford https://orcid.org/0000-0003-3106-881X
Pan Gao
Dalian Institute of Chemical Physics, Chinese Academy of Sciences
Tatchamapan Yoskamtorn
University of Oxford
Yao Xiao
Wuhan Institute of Physics and Mathematics
Sarah Day
Diamond Light Source
Chiu Tang
Diamond Light Source
Guangjin Hou
State Key Laboratory of Catalysis, Dalian Institute of Chemical Physics, Chinese Academy of Science https://orcid.org/0000-0001-8216-863X
Anmin Zheng
Innovation Academy for Precision Measurement Science and Technology, Chinese Academy of Sciences https://orcid.org/0000-0001-7115-6510
Shik Chi Tsang (✉ edman.tsang@chem.ox.ac.uk)
University of Oxford https://orcid.org/0000-0002-8796-3146

Article

Keywords: Molecular Adsorption, Crystallographic Positions, Direct Experimental Observation, Frustrated Lewis Pair, Heterolytic Molecular Reactions, Bronsted Acid Site

Posted Date: December 18th, 2020

DOI: https://doi.org/10.21203/rs.3.rs-105067/v1

License: This work is licensed under a Creative Commons Attribution 4.0 International License.
Read Full License

Abstract

There has been a long debate on how and where active sites are created for molecular adsorption and catalysis in zeolites which underpin many important industrial applications. For example, Lewis acidic site (LAS) and basic site (LBS) are generally believed to be the extra-framework Al species and residue anion (OH^-) species formed at fixed crystallographic positions on the zeolite structures after their synthesis. Here, direct experimental observation of adsorbate-induced active sites in silicoaluminophosphate (SAPO) zeolites is *for the first time* made, which contradicts the traditional view of the fixed active sites in zeolites. Evidence shows that induced Frustrated Lewis pair (three-coordinated framework Al as LAS and SiO(H) as LBS) can be transiently favored for heterolytic molecular binding/reactions of competitive polar adsorbates due to their ineffective orbitals overlap in the rigid framework. High resolution magic-angle spinning solid-state nuclear magnetic resonance (MAS-SSNMR), synchrotron X-ray diffraction (SXRD), neutron powder diffraction (NPD), in-situ Diffuse Reflectance Infrared Fourier Transform spectroscopy (in-situ DRIFT) and *ab initio* molecular dynamic (AIMD) demonstrate the presence of only one type of Bronsted acid site (BAS) in the H-SAPO-34, however, when exposed to polar adsorbates such as methanol, the methoxy moiety is shown to be directly coordinated to the framework Al (induced LAS) and the proton to the O(H)-Si (induced LBS) by the induced FLP. Our unprecedented finding opens up a new avenue to understanding of the dynamic establishment of active sites for adsorption or chemical reactions under molecular bombardments to zeolitic structures.

Main

Zeolites are the well-known solid catalysts, taking advantage of their unique molecular sieving effect, excellent catalytic activity and high thermal stability, they have been widely applied as heterogeneous catalysts in the large-scale industrial processes.[1] Even though they have enjoyed significant commercial success, many mechanistic aspects of fundamental information of zeolites are still debated, including the local structure of the acid or base centers from the atomic level. It is well accepted that zeolites are crystalline microporous frameworks consisting of corner sharing tetrahedra, connected by hinges at the oxygen atoms, the strongest forces in silica networks are those holding the rigid structural units together and also those forces bridging these tetrahedra through the twofold coordinated oxygen atoms to form a framework. Structurally, a perfectly coordinated silica network should be considered well balanced, as the number of degree of freedom exactly matches the number of constraints. This is known to be a particularly favorable situation, leading to a free-energy minimum where the strain is minimized as the network remains intact, which is also the traditional view of zeolites that are stable materials. Thus, the classical view of active sites for molecular adsorption or reaction such as Brønsted acid site (BAS) and Lewis acid site (LAS) in the Al-Si zeolites are generally believed to be on a proton attached oxygen bridge between substituted Al and Si (Si-O−(H+)-Al+) due to charge balance and extra-framework Al species, respectively formed at fixed crystallographic positions on the zeolite structures after their synthesis.

However, there are some recent intriguing observations to indicate that the framework of zeolites may not be regarded as a static structure.[2] For example, dehydroxylation of zeolite Brønsted sites at high

temperature appears to support the formation of Lewis acid sites in three-fold coordination.[3] In fact, the Si-OH-Al bridge which can be displayed as Si-O−(H+)-Al+, emphasizing the classical ion-exchange role of the proton, could also be described as SiO(H) → Al, i.e., the dative coordinative bond between a lone electron pair of SiO(H) oxygen to a three-fold coordinated Al atom, where the resonance form [4] of Brønsted and Lewis acid sites in zeolites that may thus be interconverted in principle. The flexibility of the zeolites structures has been implied by both theoretical calculations and catalytic experiments.[2,5] Treacy et al. argued that most of the existing zeolite frameworks are flexible when modeled as pure silica polymorphs.[6]

The SAPO class of zeolites has particularly attracted much attention due to its versatile catalytic properties in green chemistry, petrochemistry and refining.[7,8] Similar to normal silicoaluminum zeolites, the aluminophosphate molecular sieves consist of a tetrahedral oxide framework and the substitution of silica to them in the formation of the SAPO derivatives is described as a replacement of an (Al,P)-pair by two Si in the lattice. Altering the ratios among the Al, Si and P in different SAPO materials can generate BAS of variable quantities due to the charge compensation by protons as that of silicoaluminum. BAS over these structures is attractive for fundamental mechanistic studies, as all the active sites in H-SAPO-34 may be consider equivalent in terms of their acid strength steric accessibility, and transition state structures. However, with respect to the structure, there is a severe local distortion of the BAS T-O-T moiety from ideal tetrahedral symmetry due to the fact that the chemical nature of phosphorous is markedly dissimilar from Si and Al. Also, the local charge distribution can also play an important part in the structural distortion. Confirmed by both experiments and theoretical calculations, the distortion of bond lengths and angle of the BAS in SAPO results in a very different BAS to those in aluminosilicate zeolites.[9] Thus, the formation of Lewis acidic and basic sites from these structures during molecular adsorption/catalysis is not yet clear. By combining in-situ synchrotron-radiation X-ray powder diffraction and DFT calculations, Arstad et al.[5] demonstrated that the structure of SAPO-37 can collapse after adsorbing water molecules under 345 K. A similar observation was reported by Sliverwood et al.[10] who showed that the SAPO-34 framework contracts following ammonia adsorption by using a neutron scatting technique. Using SSNMR and DFT calculations, Morris et al.[11,12] confirmed that framework Al-O bonds in zeolites can be reversibly broken through the adsorption and desorption of water at room temperature. Very recently, Liu et al.[13] observed the same phenomenon using SSNMR. All of these observations indicate that the BAS structure is not completely stable and possesses some unquenched reactivity. However, despite these reports, it is not yet clear how and why such structural distortions occur.

On the other hand, it is recently established a frustrated Lewis pair (FLP) in homogeneous systems. This is a chemical entity containing both a Lewis acid (LA) and a Lewis base (LB) with unquenched activity at sterically hindered or rigid positions, which accordingly cannot undergo acid-base dative adduct formation. The FLP chemistry tends to take place in polar media with ionic species for the charge (electron pair) redistribution. Since the landmark report from Stephan et al.,[14] the chemistry of FLP has been successfully developed during the last decades in several multiple research systems to activate and catalyze a wide range of substrate molecules. Many new reactions have been found, and a great variety

of different FLPs have been devised, characterized, and related reactions reported. For example, they have described the syntheses of aminophosphonium salts, which incorporate Lewis basic and acidic pnictogen functionalities within an intramolecular system. These species serve as hypothetical intermediates for the generation of ring-strained amidophosphoranes via transient FLP route, which are shown to capture and sequester CO_2.[15] In contrast, few reports have been focused on the FLP chemistry in zeolites where uneven charge distribution, polar solvent stabilization, adsorbed ions may favor it to take place.

In this work, using state-of-the-art techniques such as MAS-SSNMR, SXRD, NPD, in-situ DRIFT and DFT, we report *for the first time* that Lewis acid and basic sites in SAPO zeolites can be transiently created due to induced FLP via competitive adsorption of adsorbate molecules of increasing polarity such as acetone, ethanol, methanol, and water. Instead of establishing a rigid FLP in the previous reported homogeneous systems,[16] the traditional BAS in this class of SAPO zeolites represents a quenched but less stable dative adduct (Si-O(H)-Al) due to the strains and poor orbitals overlap imposed by the rigidity of the surround framework. We postulate that due to the instability, the adduct can be broken by the introduction of a stronger Lewis basic adsorbate molecule with polarity high enough to bind to framework Al as Lewis acid where silica hydroxyl as Lewis base hence new induced LA and LB sites to intercept with the adsorbate molecules (Scheme 1). As shown in Scheme 1a, the BAS structure is maintained at a rigid static state. The HOMO is mainly located on the Al atom and the LUMO on the Si atom, with a T-O-T angle of 145° and Al-O distance of 1.84 Å. Upon adsorption of a polar molecule like methanol (Scheme 1b), the HOMO expands to envelope the methoxy species which is indicative of a methoxy-to-Al charge transfer, forming a fully quenched Al-O-CH_3 moiety. This also results in the effective cleavage of the framework Al-O bond, as observed by a highly extended inter-atomic distance (2.98 Å) and a relaxed T-O-T angle (108°). Thus, the traditional BAS was induced to form FLP sites by heterolytic binding of methanol at the stable coordinated state.

Acetone adsorption on SAPO zeolites. The supply of zeolite samples, pretreatments and detailed parameters of SSNMR experiments are given in **Supporting Information**. SSNMR is a conventional yet powerful classical tool to study Brønsted and Lewis acid sites in catalytic materials, as it provides a unique insight into structural and dynamic properties of solids at the atomic level.[17,18] Both quantitative and qualitative information at an atomic level with high resolution and sensitivity can also be achieved. Before the adsorption experiment using ^{13}C-acetone, ^{1}H, ^{27}Al, ^{29}Si, ^{31}P SSNMR characterization was performed (Figs. S3-6) which show the presence of typical BAS in the pristine samples with values agreeable to literature.[17,19,20] Curve in Fig. 1a shows the ^{13}C cross-polarization(CP) magic-angle spinning(MAS) NMR spectra of H-SAPO-34 zeolite adsorbed with ^{13}C-acetone. Interestingly, two peaks at 217 ppm (type I) and 225 ppm (type II) are clearly observed. According to the previous literature,[21] the major peak at 217 ppm is attributed to ^{13}C-acetone adsorbed on BAS. However, the other ^{13}C resonance at 225 ppm persistently appears in repeated measurements but remained ambiguous. One may consider the signal at 225 ppm to be attributed to the acetone adsorbed on the stronger BAS,[22,23] and/or acetone adsorbed at surface defects.[20] In contrast, ^{1}H, ^{27}Al, ^{29}Si, ^{31}P MAS SSNMR (Figs. S3-6) and ^{1}H-^{1}H SQ-DQ

MAS NMR (Fig. S7) spectrum of H-SAPO-34 show that only one type of BAS is present (when dried), with no framework defects observed. Furthermore, when the samples were exposed to humidity at 298 K as shown in Fig. S8, the peak intensity of the 225 ppm vanished rapidly over increasing exposure time. A similar trend was also observed in the ^{31}P signal of trimethylphosphine oxide (TMPO) pre-adsorbed on zeolites, indicating the presence of Lewis acid sites that vanish on exposure to moisture-containing air.[24] Therefore, we assigned the minor 225 ppm peak to ^{13}C-acetone adsorbed at LAS. The analysis of 2D ^{13}C-^{1}H hetero-nuclear correlation NMR spectra further supports our assignment as shown in Fig. 1d. A dominant correlation peak at (217, 12) ppm corresponding to the ^{13}C-acetone adsorbed on the BAS is anticipated; however, no correlation signal is observed between the 225 ppm and the proton of BAS (δ_H >10 ppm), with the exception of the signal at (225, 7-10) ppm. Since ^{1}H chemical shift inside zeolites at 7-10 ppm can be assigned to the hydrogen-bonded silicon hydroxyl group,[25] we assigned this signal at (225, 7-10) ppm to ^{13}C-acetone adsorbed at Lewis acid sites that are in close proximity to a hydroxyl group. The spatial relationship of 217 ppm and 225 ppm peaks was studied by 2D ^{13}C-^{13}C PDSD NMR (Fig. 1e) which shows that there is a strong cross-peak pair at (217, 225) ppm and (225, 217) ppm, indicating that the carbon atoms associated with the signals at 225 and 217 ppm are in close proximity. Thus, we have shown using SSNMR that acetone not only adsorbs primarily at BAS but the LAS as well, and that the two adsorption species are in close proximity. The dependence of the LAS on the presence of acetone is the key question to resolve.

In order to directly visualize the configurations of adsorbates in zeolites, the combination of high-resolution synchrotron X-ray powder diffraction (SXRD) and neutron powder diffraction (NPD) were adopted. It is well known that both SXRD and NPD are powerful techniques in the high resolution determination of the crystallographic positions of adsorbates, such as ammonia, methanol, carbon dioxide and ethane, in porous crystalline materials including zeolites and metal-organic frameworks.[21,26-28] Crystal structures have been refined against the diffraction data using the whole-pattern Rietveld method, yielding the spatial relationships between guest species and host frameworks. In particular, bond distances and angles at the adsorption sites were measured with acceptable experimental errors, which offers complementary information to the SSNMR analysis.

The refined structure of deuterated acetone/H-SAPO-34 is depicted in Figs. 1f-j and S12: two adsorption states are also observed that are attributed to two types of adsorption site (type-I: acetone on a BAS and type-II acetone via the induced FLP route). These coexist inside the cage with the interatomic distance between C1 in type-I acetone and C2 in type-II acetone of 5.40(2) Å(Fig.1h), which falls within the detectable range of the 2D ^{13}C-^{13}C PDSD NMR. The occupancies and atomic positions of the two species in type-I and type-II are presented in Tables S6 and S9 which match well with the NMR estimation of their amounts as 3:1. Thus, the positions and occupancies of the two adsorbed acetone states have been quantitatively defined within the unit cell and in relation to each other by both SSNMR and crystallographic methods, which are in good agreement. For the acetone type-I state, the inter-atomic angels and bond distances of Si-O(H)-Al (Al1-O3(H)-Si1:146.8°; T-O: 1.6-1.9 Å[29]) are characteristic of BAS

in H-SAPO-34, and the distance of the acetone C=O from H (BAS) of ca. 1.58(3) Å (Fig. 1i) is indicative of typical hydrogen bonding[30]. On the other hand, for acetone type-II state, the adsorption geometry of C=O is clearly leaning toward the framework Al (LAS) (Fig. 1j), exhibiting an inter-atomic distance much shorter than in acetone type-I state (2.17(4) Å vs. 3.25(7) Å). Additionally, the [Al-O-Si] bond angle of 146.8° found in typical BAS is significantly lowered to 124.3° [Al5-O4-Si2] and the Al-O bond distance is increased to 2.01(6) Å indicating the weakening of the Al-O interaction in the type-II mode (Fig. S12). These changes in geometry are attributed to some conversion of adsorption of acetone from type-I to type-II via the induced FLP route(Fig. S17). Further structural information on the unusual acetone type-II state at LAS was further observed in the dipolar interaction between the ^{13}C atom of acetone with framework ^{27}Al atoms by using ^{13}C-^{27}Al symmetry-based rotational-echo saturation-pulse double-resonance (SRESPDOR), which is based on the inter-nuclear dipolar interaction/distance (Fig. S9). Signals of 217 ppm (type-I) and 225 ppm (type-II) are both subject to a ^{13}C-^{27}Al dipolar dephasing, which clearly shows that the ^{13}C-acetone of 225 ppm is indeed in a very close proximity to the aluminum species, as shown in our refined crystal structure (Figs. 1i-j). Due to the close proximity of acetone and the Al atoms in the framework, the resonance peak at 225 ppm is subject to a more intense dipolar dephasing than that of 217 ppm. These crystallographic values match with the expectation of the induced formation of Lewis acid sites for binding of electron-donating C=O of acetone. Based on the afore-mentioned experimental evidence, new insights into the absorption states of ^{13}C-acetone over H-SAPO-34 zeolite are thus obtained (Fig. 1d left). As well as the anticipated adsorption at the typical BAS in H-SAPO-34 in which acetone adsorbs at the bridging-hydroxyl proton (217 ppm), some acetone has been shown to coordinate directly with framework Al atoms (225 ppm) from the induced FLP route.

In order to investigate the origins and driving-force behind the unusual acetone type-II state, other SAPO zeolites (H-SAPO-18 and H-SAPO-35) were studied using similar methods. Similar results were also observed in the ^{13}C chemical shifts of ^{13}C-acetone adsorbed on these samples, as shown in Figs. 1b-c. For both samples, two ^{13}C signals were also observed (H-SAPO-18: 217 ppm, 225 ppm; H-SAPO-35: 217 ppm and 227 ppm), which can be assigned to acetone adsorbed to the BAS and induced framework Al atoms (induced FLP), respectively. 2D ^{13}C-^{1}H hetero-nuclear correlation MAS NMR spectrum also support our assignment showing the correlation between carbonyl carbon and proton in BAS, i.e. (217, 12.2) ppm in H-SAPO-18 and (217, 12.7) ppm in H-SAPO-35. Meanwhile, 225 ppm (H-SAPO-18) and 227 ppm (H-SAPO-35) are correlated with the hydrogen-bonded protons (Figs. S10b and S10d). Also, according to the 2D ^{13}C-^{13}C PDSD NMR spectrum, these two ^{13}C-acetone species are close to each other (Figs. S10e-f), as was shown for H-SAPO-34. In summary, it is shown that the BAS Al-O dative bonds in SAPO zeolites can be cleaved to a degree to form induced FLP due to the adsorption of acetone by C=O binding to the Al atom. FLPs are well-known to activate small molecules, including H_2, CO_2, SO_2, NO, CO, N_2O, olefins, methanol.[31] Herein, the characterization of methanol adsorption was conducted, a more polar adsorbate

than acetone with greater availability of lone pair electrons, in order to verify whether a higher degree of induced FLP for methanol binding could be achieved in the SAPO zeolite.

Methanol adsorption on SAPO zeolites. Figs. 2a-c show the ^{13}C CP MAS SSNMR spectrum of ^{13}C-methanol adsorbed on H-SAPO-34, H-SAPO-18, and H-SAPO-35 zeolites, respectively at 298K. In contrast to acetone adsorption, in which two signals that corresponded to the two adsorption modes were deconvoluted, for methanol the Gaussian deconvolution clearly required three peaks at 50.4 ppm, 52.8 ppm and 56.4 ppm. The lowest chemical shift signal at 50.4 ppm can easily be assigned to methanol adsorbed at BAS(type-I), as it perfectly matches the literature value.[32] A small signal at 52.8 ppm, which is clearly observable on all the zeolites but almost negligible in H-SSZ-13(Fig. 2d). This can be attributed to methanol coordinated to the framework Al of BAS to form the induced FLP state(type-II), which matches to the chemical shift of CH_3O-Al species.[33] Interestingly, the 56.4 ppm peak, which corresponds to the typical NMR shift of surface methoxy species (SMS),[32] is unexpectedly obtained at room temperature. However, this may be accounted for by considering that polar methanol is vulnerable to dehydration, especially from the induced FLP state at mild conditions.

Methanol adsorption over H-SSZ-13 zeolite which processes the same structure with that of H-SAPO-34 but diffident framework composition (Si, Al, for H-SSZ-13, P, Al for H-SAPO-34) was also studied in order to investigate the role of phosphorous in the system. As shown in Fig. 2d, it exhibits very dominant adsorption as type-I, and a very low proportion of adsorbed methanol in the type-II or as SMS (52.8 and 56.4 ppm). It is noted that the typical distance of Al-O over pristine H-SSZ-13 is markedly shorter than those of the other pristine SAPO samples.[9] The shorter bond and more efficient orbital overlap forms a more stable LA-LB adduct in Al-O-Si, which is less prone to cleavage and the formation of the induced FLP and then to SMS. Thus, we show that the presence of phosphorous increases the proportion of adsorbed methanol bound both to the induced FLP and as SMS. Quite logically, it is suggested that the longer Al-O bond and unbalanced charge after phosphorus introduction are more likely to make it cleaved by the adsorption of small polar molecules, leading to the type-II state that we have comprehensively characterized by complementary crystallographic and NMR methods.

The ^{13}C-^{27}Al S-RESPDOR was then performed to qualitatively compare the distance between the methanol carbon and Al in the zeolite framework. When the recoupling time was set at 3.6 ms (Fig. 2e), the strongest dipolar ^{13}C-^{27}Al dephasing attenuation (80.5%) is observed on the 56.4 ppm peak, followed by the 52.8 ppm peak (76.5%) and then the 50.4 ppm peak (50.6%). From the simulated dephasing curve (Fig. 2f), the degrees of attenuation, which is inversely proportional to the ^{13}C–^{27}Al distance, generally match well with the experimental measurements collected at 3.6 ms (Fig. 2e). Notice that there is more than one Al atom interacting with the C-Al in proximity in the SAPO zeolites (Figs. 2j-l). This effect on the diphase ^{13}C–^{27}Al S-RESPDOR interaction makes it very difficult to derive the actual distances between the methanol carbon and Al. However, the order reflects inversely to the distance between the ^{13}C and ^{27}Al corresponding to SMS (56.4 ppm), induced FLP adsorption (52.8 ppm) and BAS adsorption (50.4 ppm), respectively.

On the other hand, for their refined crystal structures from SXRD/NPD with deuterium methanol, the geometric adsorption modes of methanol on SMS, induced FLP and BAS of H-SAPO-34 can be obtained (Figs. 2g-l and S13). Their corresponding spatial distances of methanol in type-I, type-II and SMS to each others can be directly measured as ca. 4.50(7) Å for C2-C3, 5.94(3) Å for C1-C3 and 6.47(1)Å for C1-C2, respectively (Figs. 2i and S13). According to their occupancy values (Table S8), the ratio of the peak area of methanol-BAS to summed peak areas of methanol-LA and SMS (produced from induced FLP) corresponds to ca. 1.3 ± 0.3, which is also in good agreement with the value obtained from the NMR data (Table S3). 2D ^{13}C-^{13}C PDSD NMR suggests that the dominant correlation peaks at (50.4, 56.4) ppm and (56.4, 50.4) ppm (Fig. S11) are in spatially close proximity. It is striking that in the methanol type-II adsorption geometry here (C2-methanol on Al5 in Fig. S13), the elongated Al-O bond length (2.31(8) Å) and compressed Al-O-Si angle (118.4°) are very similar to the type-II state of acetone on induced FLP as previously shown by SXRD/NPD, which appears to be greatly stretched from the typical value of 1.58(7) Å in the acetone type-I state(Fig.2j).[9] Notably, a hydrogen-bond between the H of methanol and the O of silanol is observed (H···O distance at 1.96(3)). Fig. 2e displays the schematic adsorption structures according to the refinement structures. From the refined model (Fig. S13) it is observed that SMS species (C3-methanol on Al4) after methanol dehydration is attached to Al with the shortest distance of 3.34(4)Å, which is in agreement with the analysis of the ^{13}C–^{27}Al S-RESPDOR data (Fig. 2f). Also, the framework structure (obviously excluding the bridging-'hydroxyl' proton) is typical of pristine H-SAPO-34, with an Al-O-Si angle of 145.9^{o} (Al4-O5-Si3) and typical inter-atomic distances.

There have been various discussions on the mechanism of methanol to olefin (MTO) reaction in zeolite topologies including CHA,[34] MFI,[35] Beta.[36] For the formation of SMS, it is traditionally accepted that methanol is adsorbed on BAS by a strong hydrogen-bonding interaction between the bridging-hydroxyl proton of BAS and the oxygen of methanol,[37] followed by dehydration and the loss of water (Fig. 3a left and S15). However, on normal alumino-silicate zeolites this reaction usually only occurs at high temperature (> 400 K).[38] Surprisingly, we clearly observe a small amount of methanol dehydration to SMS take place at room temperature over SAPO zeolites (Figs. 2a-c). This suggests a fundamentally different reaction pathway for this process. For SMS, it is postulated that the methoxy species is initially directly bonded to the framework Al in the induced FLP state (Fig. 3a right) with its hydroxyl proton is attached to the Lewis base site (OH). This would then favor the heterolytic cleavage of the methanol. Subsequently, a water molecule is eliminated from -SiOH_2, reforming the conventional Lewis adduct Al-O-Si yielding the SMS. It is significant that there is no C-O cleavage in the methanol in this induced FLP route since the Lewis acidic Al is anticipated to strongly bond with the Lewis basic O. This is in contrast to the conventional BAS route which likely proceeds with C-O cleavage of methanol to eliminate H_2O. Crucially, in type-I dehydration, the resulting methoxy oxygen originates from the framework; meanwhile, in type-II dehydration, the resulting methoxy oxygen originates from the methanol.

In order to verify our conjecture, in-situ DRIFT experiments were performed at elevated temperature using ^{16}O-methanol and ^{18}O-enriched methanol separately. When using non-labeled methanol the peak assigned to the stretching vibration of ^{12}C-^{16}O in methoxy species[39] appeared at 940 cm^{-1} (Fig. 3b);

meanwhile, for ^{18}O-methanol the peak is clearly shifted to 912 cm^{-1}. This indicates that the methoxy oxygen in SMS is from the methanol, and hence formed by type-II methanol adsorption. In contrast, for the typical alumino-silicate zeolite H-ZSM5 under identical conditions, there is no difference in the SMS stretching vibration when using unlabeled and ^{18}O-methanol, which indicates that the SMS methoxy oxygen is from the framework, and is formed by type-I methanol adsorption. Similarly, isotopic labeling has no effect on the peaks observed at 940 cm^{-1} and 980 cm^{-1} that were assigned to the C-^{16}O stretching vibrations of SMS in H-ZSM-5[40,41] (Fig. S16). The results discussed above provide unambiguous evidence that induced FLP adsorption of methanol can be favorably formed in SAPO zeolites justifying the superiority of H-SAPO-34 catalyst for MTO reaction, which presumably progresses through an SMS intermediate that we have empirically shown.

Theoretical calculations. To further investigate the adsorption behaviour of methanol on H-SAPO-34 zeolites, DFT calculations using VASP[42,43] and ab initio molecular dynamic (AIMD) simulations were conducted (details of calculation methods and parameters in **Supporting Information)**. The coordinating number is a value proportionate to the bonding strength with 0 corresponds to no bonding and 1 to a chemical bond. 3D diagram of coordinating numbers and energy indicate that both the classical BAS adsorption state and the induced FLP adsorption state occur when methanol is introduced into the zeolite. In general, the larger the coordinating numbers, the stronger the corresponding. As shown in Fig. 3c, O_{Zeo}-Al (initial state) and O_{MeOH}-Al (final state) coordinating numbers are 0.85 and 0.45, respectively.

An initial state of type-I BAS-adsorbed methanol in H-SAPO-34 at 1 bar and 298K was modelled by AIMD and the reaction allowed to progress at the transient time. By analyzing several inter-atomic distances it is observed that the type-I mode can be directly converted to the type-II induced FLP structure (Fig. 3d), i.e. methoxy directly bonded to the framework Al site (induced LA) and H to Si-OH site (induced LB) when temperature and pressure were taken into consideration to overcome the structural reorganization energy. Interestingly, it is shown that the conversion occurs in three distinct steps: 1) coordination of framework Al and methanolic oxygen to form a pseudo four-membered ring, 2) methanol moves close to the framework Al, and 3) cleaving of the framework Al-O bond. The process of the first step(0-14ps) to the second step(14-20ps) is observed in that the distance of the primary interaction in type-I adsorption between the bridging-hydroxyl proton and methanolic oxygen increases at 14 ps (O_{MeOH}-H_{BAS} :1.7 Å to 3.5 Å), while simultaneously the distance between Al and methanolic oxygen decreases (O_{MeOH}-Al: 3.5 Å to 2.0 Å). After that, the third step occurs in the increase of the framework Al-O distance at 20 ps (O_{SiOH}-Al: 1.9 Å to 3.2 Å) and further decrease of the distance for O_{MeOH}-Al (2.0 Å to 1.9 Å)and O_{MeOH}-H_{BAS}(3.5 Å to 2.9 Å). Here it is shown by computational methods that conversion between there type-I and type-II adsorption mode is possible and occurs through a pseudo four-membered ring intermediate state. Similar results were also obtained based on acetone adsorption calculations (Fig. S17).

A further fundamental question is how the nature of the adsorbate molecule affects type-II induced FLP adsorption and their related product. By using the increasingly polar adsorbates, acetone, ethanol, methanol and water as the NMR probe molecules, the K ratio of the normalized type II peaks (induced

FLP + surface-alkoxy species) in reference to the total adsorbate by integrating their peak areas from the NMR data are given (Table S3). Interestingly, we have discovered a linear relationship between the adsorbate polarity and their relative amount in the K ratio (Fig. 3e, red). The calculated FLP free energy changes are logarithmic correlated with the polarity, in which high polarity adsorbates giver lower reorganization energy required to the induced FLP state from BAS state (Fig. 3e, purple). Undoubtedly, the thermodynamic preference for binding by cleaved Al as LA against O(H)Si in the induced FLP is highly dependent on the polarity of the molecule because greater availability of the adsorbate electron pair leads to greater Lewis basicity and reactivity with the LA Al site. The entropic contribution, solvency as well as charge stabilization in H-SAPO-34 are envisaged to overcome the lower reorganization energy and facilitate the FLP route from BAS. In summary, the more polar the adsorbate, the greater the proportion of adsorbate is bound in the type-II state and the stronger this binding is.

We have also excitingly found a correlation between the initial Al-O(H)-Si bond angle and the adsorption energy of methanol. The energies of various H-SAPO-34 clusters with fixed Al-O-Si bond angles between 120 and 150° were optimized using DFT calculations. We show that the greater the distortion from the typical zeolite angle of 145° results in linearly decreasing adsorption strength (Fig. 3f). The larger T-O-T angle gives higher adsorption energies. It means that BAS sites with the conventional zeolitic angle are easier to convert to induced FLP sites by competitive molecular adsorption and catalysis, relative to more distorted SAPO zeolites. We also anticipate that increasing temperature could increase the proportion of adsorption resulting in FLP geometry through type-I to type-II conversion, but further work is required to characterize the temperature dependence of these structures and overall system.

There is no doubt from the literature that Lewis acid/basic sites can be created in zeolites, such as by the introduction of hetero-atoms during synthesis or extra-framework Al species during de-alumination. Poncelet et al.[44] reported three types of Al species in Beta which can be inter-transformed to each other. Koningsberger et al.[45] subsequently confirmed their presence by using in situ X-ray absorption near-edge spectroscopy. Dedecek et al.[46] demonstrated the formation of $(SiO)_3Al$ from the de-hydroxylation of $(SiO)_3AlOH$ in CHA zeolite. These moieties are clearly in pre-existence for characterization but are very reactive and may be subject to site poisoning in handling. In this work, we have demonstrated that induced FLP sites are created by small molecule adsorption/activation over H-SAPO zeolites. It is difficult to characterize the structure of the induced FLP sites during catalysis due to the challenge of collecting experimental data under fast dynamic reaction conditions or exposure of the system to reaction mixture with complex matrix. However, we believe that the observation of this new binding mode can offer great insights into existing systems and exciting new prospects in transient catalysis in the future.

In summary, the combination of state-of-the-art solid state NMR experiments, synchrotron X-ray powder diffraction, neutron powder diffraction, in-situ DRIFT and theoretical calculations has revealed the formation of transient active sites for adsorption/catalysis of small molecules. The classical view of rigid and stable zeolite materials with pre-existing active sites is not a complete description. Instead, we propose that zeolite structures could be labile, dynamic and fluxional due to ineffective orbitals overlap in

distorted environments which make the structures responsive to environment. With regard to the catalytic implications, we demonstrate that the presence of induced FLP acid sites offers a new route to form the key surface-methoxy intermediate in methanol-to-olefin reactions over SAPO catalysts. This observation may provide mechanistic information for the design and characterization of the in-situ generation of catalytic sites in other materials and for other catalysis reactions under tailored reaction mixture.

Methods

Solid-state NMR

1 Dimensional (D) ^{1}H magic Angle Spinning(MAS) NMR measurements were carried out using a Bruker Avance III 400 WB spectrometer at resonance frequencies of 399.33 MHz. ^{1}H MAS NMR spectra were acquired on a 4 mm probe with a spinning rate of 10 kHz, a π/2 pulse length of 3.8 μs, and a recycle delay of 5 s, while the samples used for the ^{1}H MAS NMR studies were additionally dehydrated in vacuum at 673 K for 10 h before the measurements or the loading with the adsorption molecules.

2D ^{1}H-^{1}H single quantum-double quantum (SQ-DQ) MAS NMR experiments, double-quantum coherences were excited and reconverted with the R12 pulse sequence with ν_{1H} = 3 ν_R= 37.5 kHz, and the excitation and reconversion time were set to 0.48 ms. The increment interval in the indirect dimension was set to 80 μs, and 72 t1 increments and 180 scan accumulations for each t1 increment were used.

^{27}Al, ^{29}Si, ^{31}P MAS NMR experiments were carried out on a Varian InfinityPlus-300 spectrometer with the Larmor frequencies of 78.16, 59.59, 121.50 MHz, respectively. ^{27}Al MAS NMR spectra were recorded with a pulse length of 0.2 μs (<π/12), a recycle delay of 1 s, and a spinning rate of 10 kHz. ^{29}Si MAS NMR spectra with high-power proton decoupling were recorded on a 7.5 mm probe with a spinning rate of 3.5 kHz, a π/2 pulse length of 5.2 μs, and a recycle delay of 80 s. Unlike the ^{1}H and ^{13}C NMR spectra, which were obtained from dehydrated samples, the ^{27}Al and ^{29}Si MAS NMR investigations were carried out with samples that were fully hydrated at ambient temperature overnight in a desiccator. ^{31}P MAS NMR spectra were recorded with a pulse length of 4.6 μs (π/2), a recycle delay of 3 s, and a spinning rate of 10 kHz.

1D ^{13}C cross-polarization (CP) and all the 2D MAS NMR experiments were performed on Bruker Avance III 400 WB spectrometer at resonance frequencies of 104.22 MHz. ^{13}C CP MAS NMR were acquired on a 4 mm probe with a contact time of 4 ms, a recycle delay of 2.5 s, and a sample spinning rate of 10 kHz.

2D ^{13}C-^{13}C proton-driven spin diffusion (PDSD) MAS NMR experiments were performed to determine the correlations between ^{13}C signals. ^{1}H→^{13}C cross polarization with a contact time of 4.8 ms was used to prepare the initial ^{13}C signal. The π/2 pulse width of ^{13}C is 4.9 μs and the mixing time was set to 100 ms. A TPPM-13 ^{1}H decoupling at 62.5kHz was applied to the acquisition time t2. The experiments were acquired with 64 scans per experiment and 360 experiments in the State-TPPI scheme.

2D ^{13}C-^{1}H hetero-nuclear correlation MAS NMR experiments were carried out with a contact time of 4.8 ms and with a repetition time of 2 s. The Hartmann–Hahn condition was optimized by using hexamethylbenzene. High-power broad band ^{1}H decoupling, using the pulse scheme TPPM-13 with the amplitude of 62.5 kHz, was applied during ^{13}C signal acquisition to enhance spectral resolution and sensitivity.

^{13}C-^{27}Al symmetry-based rotational-echo saturation-pulse double-resonance (SRESPDOR) MAS NMR experiments were carried out with the help of a frequency splitter (REDOR-BOX), which enables tuning and matching to the Larmor frequencies of the ^{13}C and ^{27}Al nuclei on the X channel of 4mm HXY MAS NMR probe at the same time. The pulse sequence of ^{13}C-^{27}Al RESPDOR is shown in Scheme S1. The initial ^{13}C signal was prepared by $^{1}H \rightarrow {}^{13}C$ cross polarization (same condition as the previous ^{1}H-^{13}C CP MAS experiments). SR4 dipolar recoupling was used on the ^{13}C channel with $n_{nut,13C}$ =20 kHz. Continuous-wave ^{1}H decoupling with the amplitude of 62.5 kHz was used during SR4, while a SPINAL-64 (small-phase incremental alternation with 64 steps) ^{1}H decoupling with the amplitude of 62.5 kHz was used during acquisition. A π pulse length of 8 μs was used on the ^{13}C channel. The saturation pulse on the ^{27}Al channel was divided into two pulses with duration of 75 μs (0.75 Tr) to transfer ^{13}C-^{27}Al interactions. Since the S-RESPDOR experiment is extremely sensitive to the resonance offset, the ^{13}C irradiation frequency was placed in the center of the observed signals (52 ppm), and the saturation pulse on the ^{27}Al channel was irradiating at 50.6 ppm, which corresponds to the tetrahedral framework Al of the H-SAPO-34 zeolite. The recycle delay was set to 3 s.

Synchrotron powder X-ray diffraction (SXRD) and Neutron powder diffraction (NPD)

SXRD data were collected at Beamline I11, Diamond Light Source, Harwell, UK. The energy of the incident X-ray flux was set at 15 keV. The wavelength and 2θ-zero point were refined using a diffraction pattern obtained from a high-quality silicon powder (SRM640c). For the parent sample, H-SAPO-34 was ground and loaded in a 0.5 mm borosilicate glass capillary and then activated under vacuum at 423 K for 2 h. For the methanol-loaded and acetone-loaded samples, each sample was degassed at 473 K for 3 h under reduced pressure using a Schlenk line. The sample was then naturally cooled down to the room temperature. The sample was loaded into a quartz-type capillary with a diameter of 0.5 mm and sealed perfectly by using a flame. High-resolution SXRD data were obtained from the zeolite samples using the multi-analyser crystals (MAC) detectors. The patterns were collected in the 2θ range 0-150° with 0.003° data binning. Each MAC pattern was collected for 20 mins for good statistics.

NPD data were collected at beamline “the general purpose powder diffractometer” (GDDP), China Spallation Neutron Source (CSNS), Dongguan, China, using the time-of-flight diffractometer GPPD. Before a NPD data collection, H-SAPO-34 was dehydrated under vacuum at 573K for 24 h to remove the adsorbed water and other impurity gas molecules on the vacuum line. After cooling to the room temperature, a known amount of D_4-methanol and D_6-acetone were introduced into the samples named with D_4-methanol/H-SAPO-34 and D_6-acetone/H-SAPO-34, respectively. A sample was loaded in a

vanadium can with 9.1 mm in diameter in a glove box. The wavelength (l = 1.4940(1) and 1.8856(1) Å) and the 2θ zero point (2θ = -0.02269^{o}) were determined by fitting the diffraction data of a high-quality $Na_2Al_2Ca_3F_{14}$ sample. The diffraction patterns were scanned for 4 hours for good statistics.

In situ Diffuse Reflectance Infrared Fourier Transform (DRFIT) spectroscopy experiments

In situ DRFIT experiments were performed on Nicolet iS50 FT-IR spectrometer with a high temperature, high pressure DRIFT reaction cell using an MCT/A detector and at a resolution of 4 cm^{-1}.

In situ DRIFT of methanol adsorption experiments, 50 mg H-SAPO-34 zeolites (after calcination in air at 823K for 6 h) was first activated in pure N_2 flow (10 mL/min) at 673K (with linear heating to 673K for 2 h and holding for 2 h). Following, the system was cooled down to room temperature. After taking the background spectrum under N_2 atmosphere at room temperature, a constant N_2 flow 5% (10 mL/min) were introduced into a ^{16}O-methanol/^{18}O-methnaol solution for bubbling 2 mins. Then heating up to 523K hold for 3 mins for reaction. After that, N_2 was introduced into the system again to purge the extra-adsorbed species and cool down to the room temperature for scanning. Each spectra was scanned 64 times. For DRIFT of H-ZSM-5 zeolite, all the procedures are same with that of H-SAPO-34, except that the temperature of data collection in the range of 373K to 523K.

Density Functional Theory (DFT) calculations

The structural optimization presented in this work were performed using VASP software. The generalized gradient approximation (GGA) under the scheme proposed by Perdew, Burke and Ernzerhof (PBE) was used, Grimme's method was added to the GGA energy to account for the long range-interactions (DFT-D3). The projector augmented wave (PAW) was used to describe electron-ion interaction with the plane wave basis set kinetic energy cutoff equal to 500 eV. The sampling of Brillouinzone was only with Gamma point (1x1x1). The convergence criterion for the electronic self-consistency measured by the change in the total energy between successive iterations was set to 10^{-5} eV/u.c. All the atomic positions was relaxed within a conjugate-gradient algorithm until all the forces acting on the atoms were lower than 0.03 eV/ Å.

All the AIMD simulations were employed by CP2K software, and the linked PLUMED code was used to carry out the MTD simulations. The PBE functional with consideration of Grimme's D3 dispersion corrections was chosen for the DFT calculations. The double-ζ valence plus polarization DZVP basis set and Goedecker-Teter-Hutter (GTH) pseudopotential was used for the system. During the SCF procedure, a 360 Ry density CUTOFF criterion with the finest grid level was employed, together with multi-grids number 4 (NGRID 4 and REL CUTOFF 70). The temperature of AIMD was controlled by a chain of five Nosé-Hoover thermostats, and the integration time step was set to 0.5 fs.

Declarations

Acknowledgments

The diffraction and refinement works and part of NMR studies were taken place at the University of Oxford, UK funded under the IUK- EPSRC grant (55872-383337) with the SXRD and NPD beamtimes (P2018121100019) allocated by Diamond Synchrotron Light Source, UK and China Spallation Neutron Source, respectively. Supports were also obtained by the National Natural Science Foundation of China (No. 22032005, 21802164, 21902180, 21991092, and 22002174). Natural Science Foundation of Hubei Province of China (2018CFA009), and Key Research Program of Frontier Sciences, CAS (QYZDB-SSW-SLH026). GL gratefully thanks the financial support from China Scholarship Council (Grant No. 201804910472) to enable him to work at the University of Oxford. CF acknowledges the EPSRC-Diamond Light Source joint DPhil Scholarships, UK and for SXRD beamtimes for this work.

Contributions

G. L., P. Z. performed the NPD experiments and C. F., S. D., C.T. carried out the SXRD experiments. G. L., C. F., P. Z., T. Y. then analysed the SXRD and NPD data. G. L., P. G., G. H. collected and analysed the data of solid state NMR. G. L., X. Y., W. C., Y, X., conducted the DFT calculations. A. Z. and E. T. designed the experiments and G. L., E.T., wrote the paper with input from all other authors. All authors participated in the interpretation of the data and the discussions.

Corresponding authors

Correspondence to Prof. S.C. Edman Tsang and Prof. Anmin Zheng

Emails: edman.tsang@chem.ox.ac.uk (S. C. E. Tsang) and zhenganm@wipm.ac.cn (A. M. Zheng)

Ethics declarations

Competing interests

The authors declare no competing interests.

References

1 Kulprathipanja, S. *Zeolites in industrial separation and catalysis*. 1-26 (John Wiley & Sons, 2010).

2 Sartbaeva, A., Wells, S. A., Treacy, M. & Thorpe, M. The flexibility window in zeolites. *Nat. Mater.* **5**, 962-965 (2006).

3 Bolton, A. & Lanewala, M. A mechanism for the isomerization of the hexanes using zeolite catalysts. *J. Catal.* **18**, 1-11 (1970).

4 Barthomeuf, D., Derouane, E. G. & Hölderich, W. *Guidelines for mastering the properties of molecular sieves: relationship between the physicochemical properties of zeolitic systems and their low dimensionality*. Vol. 221 (Springer Science & Business Media, 2013).

5 Kalantzopoulos, G. N. *et al.* Factors Determining Microporous Material Stability in Water: The Curious Case of SAPO-37. *Chem. Mater.* **32**, 1495-1505 (2020).

6 Kapko, V., Dawson, C., Treacy, M. & Thorpe, M. Flexibility of ideal zeolite frameworks. *Phys. Chem. Chem. Phys.* **12**, 8531-8541 (2010).

7 Tian, P., Wei, Y., Ye, M. & Liu, Z. Methanol to Olefins (MTO): From Fundamentals to Commercialization. *ACS Catal.* **5**, 1922-1938, doi:10.1021/acscatal.5b00007 (2015).

8 Haw, J. F., Song, W., Marcus, D. M. & Nicholas, J. B. The Mechanism of Methanol to Hydrocarbon Catalysis. *Acc. Chem. Res.* **36**, 317-326, doi:10.1021/ar020006o (2003).

9 Sastre, G., Lewis, D. W. & Catlow, C. R. A. Structure and stability of silica species in SAPO molecular sieves. *J. Phys. Chem.* **100**, 6722-6730 (1996).

10 Silverwood, I. P. SAPO-34 Framework Contraction on Adsorption of Ammonia: A Neutron Scattering Study. *ChemPhysChem* **20**, 1747-1751 (2019).

11 Heard, C. J. *et al.* Fast room temperature lability of aluminosilicate zeolites. *Nat. Commun.* **10**, 1-7 (2019).

12 Pugh, S. M., Wright, P. A., Law, D. J., Thompson, N. & Ashbrook, S. E. Facile, Room-Temperature 17O Enrichment of Zeolite Frameworks Revealed by Solid-State NMR Spectroscopy. *J. Am. Chem. Soc.* **142**, 900-906 (2019).

13 Sun, T. *et al.* Water-Induced Structural Dynamic Process in Molecular Sieve under Mild Hydrothermal Conditions: A Novel Ship-in-Bottle Strategy for Acidity Identification and Catalyst Modification. *Angew. Chem. Int. Ed. Engl.* **59**, 2-12 (2020).

14 Stephan, D. W. The broadening reach of frustrated Lewis pair chemistry. *Science* **354**, aaf7229 (2016).

15 Hounjet, L. J., Caputo, C. B. & Stephan, D. W. Phosphorus as a Lewis acid: CO2 sequestration with amidophosphoranes. *Angewandte Chemie International Edition* **51**, 4714-4717 (2012).

16 Stephan, D. W. & Erker, G. Frustrated Lewis pair chemistry: development and perspectives. *Angew. Chem. Int. Ed. Engl.* **54**, 6400-6441 (2015).

17 Hunger, M. Multinuclear solid-state NMR studies of acidic and non-acidic hydroxyl protons in zeolites. *Solid State Nucl. Magn. Reson.* **6**, 1-29, doi:10.1016/0926-2040(95)01201-x (1996).

18 Zheng, A., Liu, S.-B. & Deng, F. P-31 NMR Chemical Shifts of Phosphorus Probes as Reliable and Practical Acidity Scales for Solid and Liquid Catalysts. *Chem. Rev.* **117**, 12475-12531, doi:10.1021/acs.chemrev.7b00289 (2017).

19 Muller, M., Harvey, G. & Prins, R. Quantitative multinuclear MAS NMR studies of zeolites. *Micropor. Mesopor. Mat.* **34**, 281-290, doi:10.1016/s1387-1811(99)00180-8 (2000).

20 Buchholz, A., Wang, W., Xu, M., Arnold, A. & Hunger, M. Thermal stability and dehydroxylation of Bronsted acid sites in silicoaluminophosphates H-SAPO-11, H-SAPO-81 H-SAPO-31, and H-SAPO-34 investigated by multi-nuclear solid-state NMR spectroscopy. *Micropor. Mesopor. Mat.* **56**, 267-278, doi:10.1016/s1387-1811(02)00491-2 (2002).

21 Zhao, P. *et al.* Entrapped single tungstate site in zeolite for cooperative catalysis of olefin metathesis with Brønsted acid site. *J. Am. Chem. Soc.* **140**, 6661-6667 (2018).

22 Martins, G. *et al.* Revisiting the nature of the acidity in chabazite-related silicoaluminophosphates: combined FTIR and 29Si MAS NMR study. *J. Phys. Chem. C* **111**, 330-339 (2007).

23 Shen, W. *et al.* A study of the acidity of SAPO-34 by solid-state NMR spectroscopy. *Micropor. Mesopor. Mat.* **158**, 19-25, doi:10.1016/j.micromeso.2012.03.013 (2012).

24 Wiper, P. V., Amelse, J. & Mafra, L. Multinuclear solid-state NMR characterization of the Brønsted/Lewis acid properties in the BP HAMS-1B (H-[B]-ZSM-5) borosilicate molecular sieve using adsorbed TMPO and TBPO probe molecules. *J. Catal.* **316**, 240-250 (2014).

25 Schroeder, C. *et al.* Hydrogen Bond Formation of Brønsted Acid Sites in Zeolites. *Chem. Mater.* **32**, 1564-1574 (2020).

26 Lo, B. T. *et al.* Elucidation of Adsorbate Structures and Interactions on Brønsted Acid Sites in H-ZSM-5 by Synchrotron X-ray Powder Diffraction. *Angew. Chem. Int. Ed. Engl.* **128**, 6085-6088 (2016).

27 Lo, B. *et al.* Dynamic modification of pore opening of SAPO-34 by adsorbed surface methoxy species during induction of catalytic methanol-to-olefins reactions. *Appl. Catal. B* **237**, 245-250 (2018).

28 Zhao, P. *et al.* Structural dynamics of a metal–organic framework induced by CO 2 migration in its non-uniform porous structure. *Nat. Commun.* **10**, 1-8 (2019).

29 Jeanvoine, Y., Ángyán, J. G., Kresse, G. & Hafner, J. Brønsted acid sites in HSAPO-34 and chabazite: an ab initio structural study. *J. Phys. Chem. B* **102**, 5573-5580 (1998).

30 Li, G. *et al.* A nonpolar solvent effect by CH/interaction inside zeolites: characterization, mechanism and concept. *Commun. Chem.* **54**, 13435-13438, doi:10.1039/c8cc08310j (2018).

31 Stephan, D. W. Frustrated Lewis pairs: from concept to catalysis. *Acc. Chem. Res.* **48**, 306-316 (2015).

32 Wang, W. & Hunger, M. Reactivity of surface alkoxy species on acidic zeolite catalysts. *Acc. Chem. Res.* **41**, 895-904 (2008).

33 Wang, C. *et al.* Extra-Framework Aluminum-Assisted Initial C– C Bond Formation in Methanol-to-Olefins Conversion on Zeolite H-ZSM-5. *Angew. Chem. Int. Ed. Engl.* **130**, 10354-10358 (2018).

34 Zhu, Q. *et al.* The study of methanol-to-olefin over proton type aluminosilicate CHA zeolites. *Micropor. Mesopor. Mat.* **112**, 153-161 (2008).

35 Goguen, P. W. *et al.* Pulse-quench catalytic reactor studies reveal a carbon-pool mechanism in methanol-to-gasoline chemistry on zeolite HZSM-5. *J. Am. Chem. Soc.* **120**, 2650-2651, doi:10.1021/ja973920z (1998).

36 Zhao, X. B. *et al.* Investigation of methanol conversion over high-Si beta zeolites and the reaction mechanism of their high propene selectivity. *Catal. Sci. Technol.* **7**, 5882-5892, doi:10.1039/c7cy01804e (2017).

37 Shah, R., Payne, M., Lee, M.-H. & Gale, J. D. Understanding the catalytic behavior of zeolites: A first-principles study of the adsorption of methanol. *Science* **271**, 1395-1397 (1996).

38 Jiang, Y. J., Hunger, M. & Wang, W. On the reactivity of surface methoxy species in acidic zeolites. *J. Am. Chem. Soc.* **128**, 11679-11692, doi:10.1021/ja061018y (2006).

39 Qian, Q. *et al.* Combined Operando UV/Vis/IR Spectroscopy Reveals the Role of Methoxy and Aromatic Species during the Methanol-to-Olefins Reaction over H-SAPO-34. *ChemCatChem* **6**, 3396-3408 (2014).

40 Matam, S. K., Howe, R. F., Thetford, A. & Catlow, C. R. A. Room temperature methoxylation in zeolite H-ZSM-5: an operando DRIFTS/mass spectrometric study. *Commun. Chem.* **54**, 12875-12878 (2018).

41 Matam, S. K., Nastase, S. A., Logsdail, A. J. & Catlow, C. R. A. Methanol loading dependent methoxylation in zeolite H-ZSM-5. *Chem. Sci.* **11**, 6805-6814 (2020).

42 Kresse, G. & Furthmüller, J. Efficiency of ab-initio total energy calculations for metals and semiconductors using a plane-wave basis set. *Comput. Mater. Sci.* **6**, 15-50 (1996).

43 Kresse, G. & Furthmüller, J. Efficient iterative schemes for ab initio total-energy calculations using a plane-wave basis set. *Phys. Rev. B* **54**, 11169 (1996).

44 Collignon, F., Jacobs, P. A., Grobet, P. & Poncelet, G. Investigation of the Coordination State of Aluminum in β Zeolites by X-ray Photoelectron Spectroscopy. *J. Phys. Chem. B* **105**, 6812-6816, doi:10.1021/jp0106202 (2001).

45 van Bokhoven, J. A., van der Eerden, A. M. J. & Koningsberger, D. C. Three-Coordinate Aluminum in Zeolites Observed with In situ X-ray Absorption Near-Edge Spectroscopy at the Al K-Edge: Flexibility of Aluminum Coordinations in Zeolites. *J. Am. Chem. Soc.* **125**, 7435-7442, doi:10.1021/ja0292905 (2003).

46 Brus, J. *et al.* Structure of Framework Aluminum Lewis Sites and Perturbed Aluminum Atoms in Zeolites as Determined by Al-27{H-1} REDOR (3Q) MAS NMR Spectroscopy and DFT/Molecular Mechanics. *Angew. Chem. Int. Ed. Engl.* **54**, 541-545, doi:10.1002/anie.201409635 (2015).

Scheme

Scheme 1 is available in the Supplementary Files.

Figures

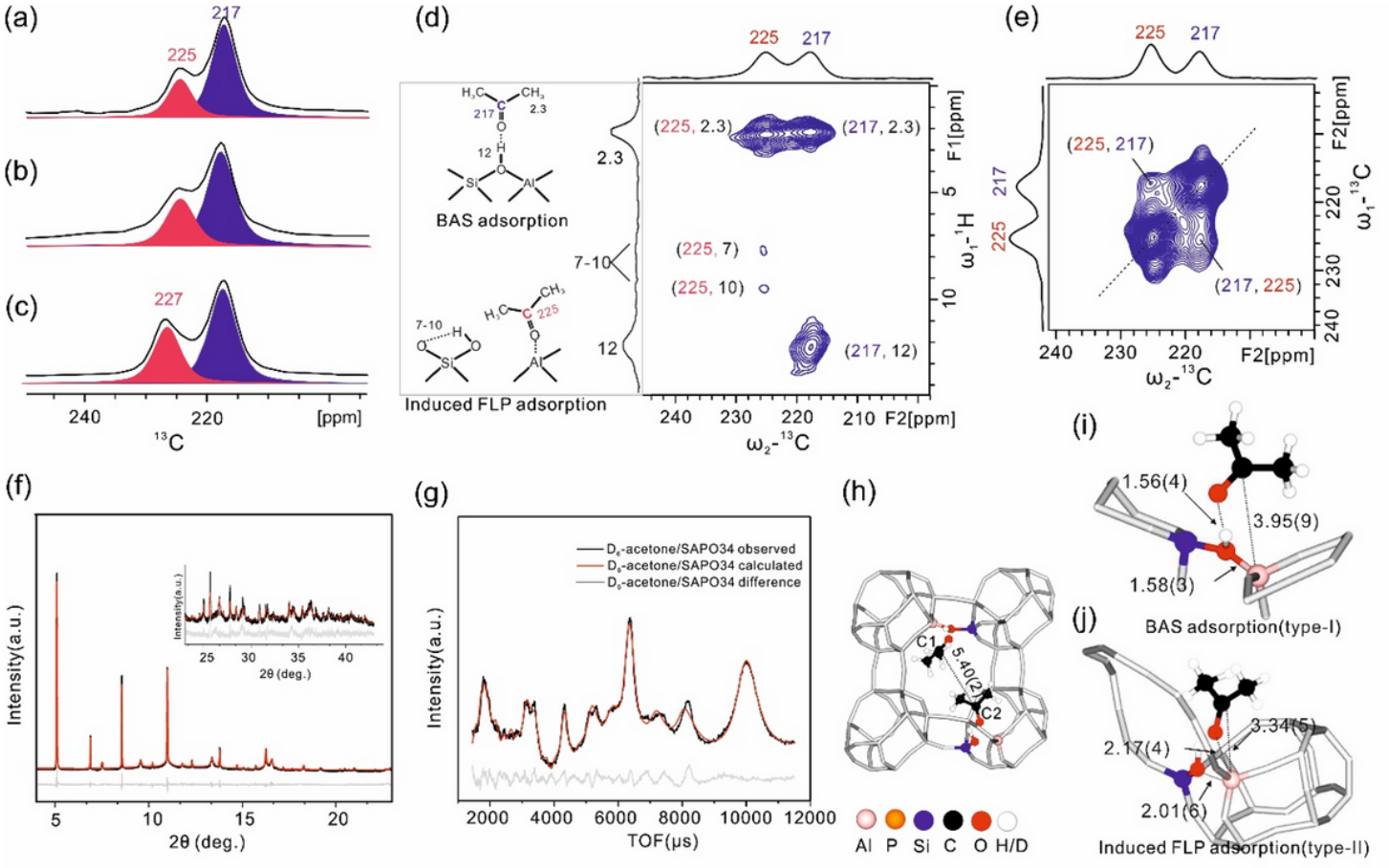

Figure 1

Adsorption structures of acetone over H-SAPO-34. 13C Cross-Polarization MAS NMR spectrum of 13C-acetone adsorbed on H-SAPO-34 (a), H-SAPO-18 (b), H-SAPO-35 (c), 2D 13C-1H hetero-nuclear correlation MAS NMR spectra with a contact time of 4 ms in right of (d), Schematic depicts the proposed the signals assignment of acetone BAS and induced FLP adsorptions in left of (d) and 13C-13C proton-driven spin

diffusion MAS NMR spectra of 13C-acetone adsorbed on SAPO-34 zeolite(e), all the data were collected on Bruker Avance III 400 WB spectrometer using 4mm rotor at a spinning speed of 10 kHz at 298K. Data analysis was performed on Bruker TopSpin. SXRD data measured at 298 K of acetone in H-SAPO-34 (Rwp = 8.9%, χ2 = 1.97) (f), NPD data measured at 298K of D6-acetone in H-SAPO-34 (Rwp = 1.9%, χ2 = 2.27) fitted by Rietveld refinement in TOPAS Academic 6 (g), SXRD data in the range of 25-45° are expanded to illustrate the quality of Rietveld refinement. Due to the low scattering of light elements such as H by SXRD, NPD was adopted to determine the H/D location. Crystallographic model based on both SXRD and NPD Rietveld refinement (see Fig. S12 for further details) (h), acetone adsorbed on BAS, type-I(i) and the framework Al site, type-II (symmetry in adsorption sites is disregarded for clarity. The atomic and crystallographic parameters are summarized in Tables S4, 6, 7, 9), (j).

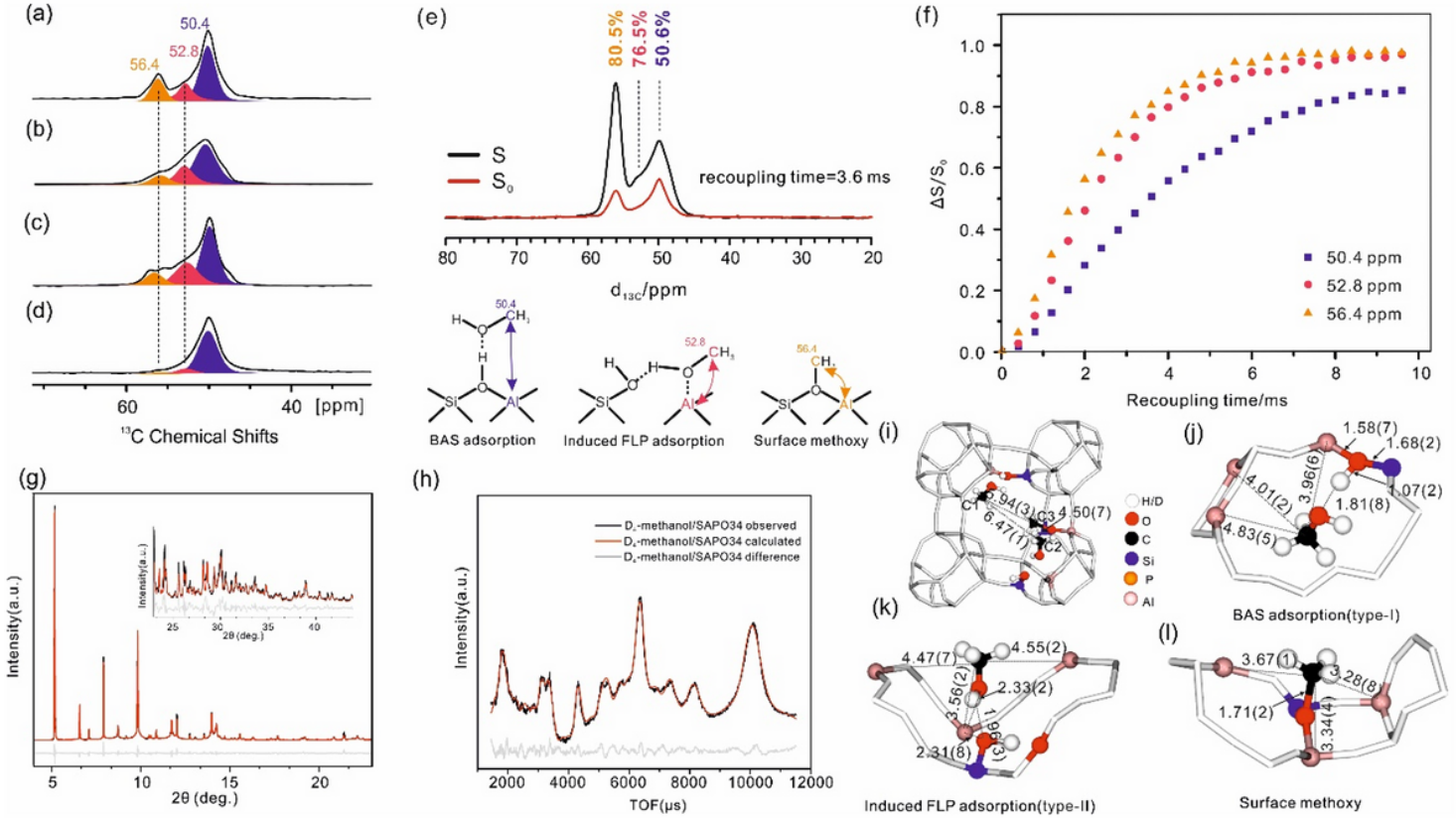

Figure 2

Adsorption structures of methanol over H-SAPO-34. 13C Cross-Polarization MAS NMR spectrum of 13C-methanol adsorbed on H-SAPO-34(a), H-SAPO-18(b), H-SAPO-35(c), H-SSZ-13(d), 13C-27Al-S-RESPDOR spectra of 13C-methanol adsorbed on H-SAPO-34 in top of (e), Schematic depicts the proposed the signals assignment of BAS adsorption, FLP adsorption and the surface methoxy species in bottom of (e), 13C-27Al-S-RESPDOR built-up data of signals at 50.4 ppm(purple square), 52.8 ppm(red dots) and 56.4 ppm(yellow triangle)(f), all the data were collected on Bruker Avance III 400 WB spectrometer using 4mm rotor at a spinning speed of 10 kHz at 298K. Data analysis was performed on Bruker TopSpin. SXRD data measured at 298K of methanol in H-SAPO-34 (Rwp = 9.4%, χ2 = 10.34) (g), NPD data measured at 298K of D4-methanol in H-SAPO-34 (Rwp= 1.4%, χ2 = 1.6) fitted by Rietveld refinement in TOPAS Academic 6

(h). SXRD data in the range of 25-45° are zoomed to illustrate the quality of Rietveld refinement. Due to the invisibility of light elements like H by SXRD, NPD was adopted to detect the H/D location. Crystallographic model based on both SXRD and NPD Rietveld refinement (i), methanol adsorbed on BAS, type I (j) and the framework Al site, type II (k), and the formed surface methoxy species (see Fig. S13 for further detail), (l). Symmetry in adsorption sites is disregarded for clarity. The atomic and crystallographic parameters are summarized in Tables S4, 5, 6, 8.

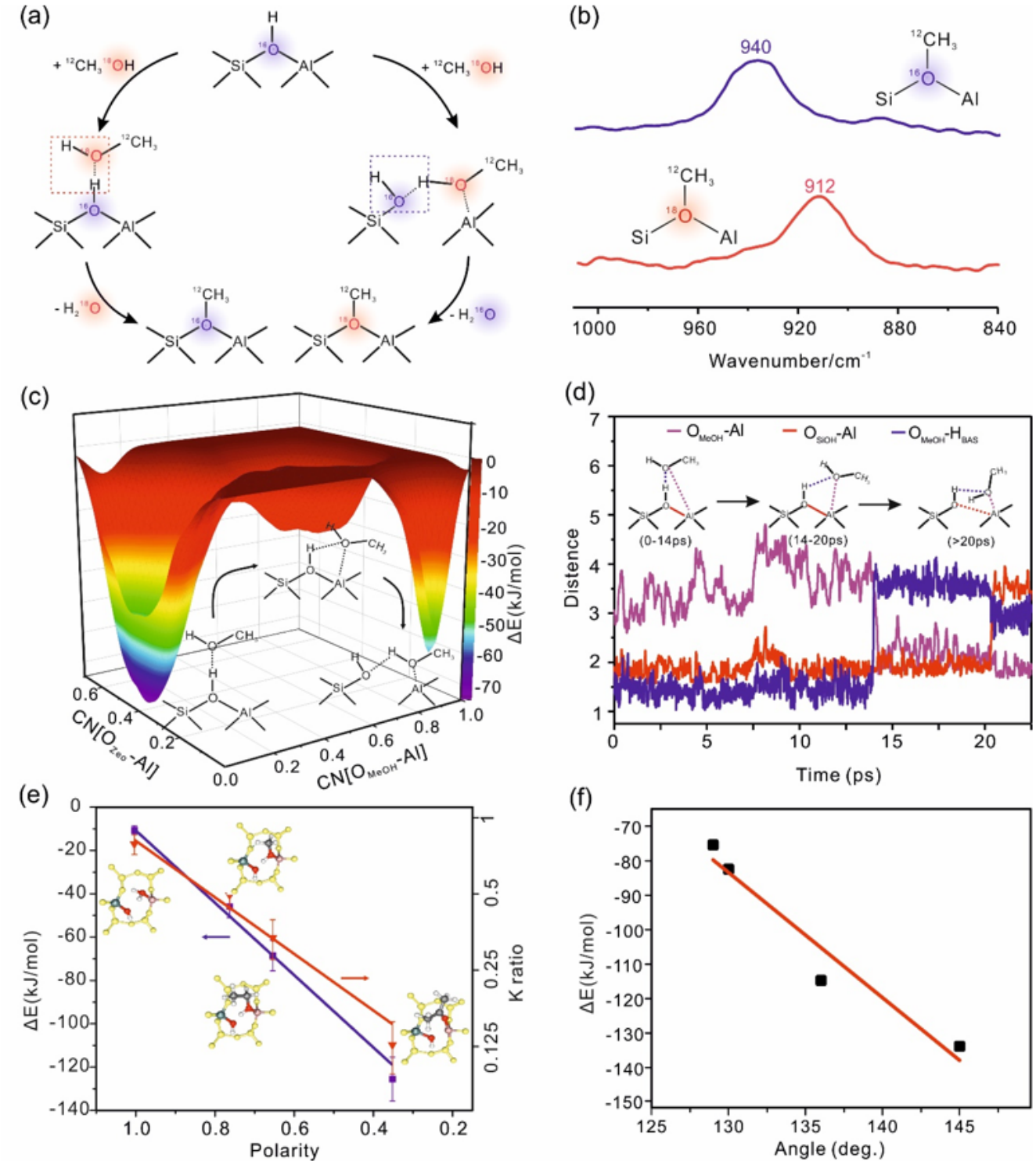

Figure 3

In situ DRIFT and DFT Calculations. Schematic depicts the mechanisms of the formation of surface methoxy species via the traditional BAS route and our proposed induced FLP route (a), in-situ DRIFT experiments showing the C-O stretching vibration peak position of methoxy species for samples of 16O-methanol/H-SAPO-34(purple) and 18O-methanol/H-SAPO-34(red) (the data were collected on Nicolet iS50 FT-IR spectrometer with a high temperature, high pressure DRIFT reaction cell using an MCT/A detector, 64 scans and at a resolution of 4 cm-1) (b), 3D diagram of the coordinating number changes for methanol adsorbed on H-SAPO-34 with the transformation from BAS adsorption state to induced FLP adsorption state during the AIMD simulations x-axis: coordinating number of OMeOH-Al (CN[OMeOH-Al]); y-axis: coordinating number of OZeo-Al (CN[OZeo-Al]), z-axis: free energy change of various states from high to low in kJ/mol (red to purple) (c), the changes of bond distance for methanol adsorbed on H-SAPO-34 with the transformation from initial BAS adsorption state to induced FLP adsorption state during the AIMD simulations Purple: distance between O of methanol and framework Al(OMeOH-Al), Red: distance between O and Al of BAS(OSiOH-Al), purple: distance between O of methanol and H of BAS(OMeOH-HBAS) (d), the free energy change (adsorption state - ground state, blue line) and K ratio (type-II+ surface-alkoxy)/(all adsorption states) – red line) of H-SAPO-34 as the function of polarity of various adsorbates (acetone, ethanol , methanol, water) (e), the relationship between free energy change and hypothetical angles of BAS (Al-O(H)-Si) of H-SAPO-34 zeolite (f).

Supplementary Files

This is a list of supplementary files associated with this preprint. Click to download.

- FLPSInaturechem.docx
- Scheme1.png